Robust Classification Scheme for Airplane Targets With Low Resolution Radar Based on EMD-CLEAN Feature Extraction Method

Lan Du, *Member, IEEE*, Baoshuai Wang, Yanbing Li, and Hongwei Liu, *Member, IEEE*

***Abstract*— A novel classification scheme is proposed to categorize airplane targets into three kinds, *i.e.*, turbojet aircraft, prop aircraft, and helicopter based on the jet engine modulation (JEM) characteristics of their low resolution radar echoes. From the pattern classification viewpoint, the low-dimensional feature vector is extracted via a two-step feature extraction algorithm based on empirical mode decomposition method and CLEAN technique. The feature extraction method can separate the fuselage component and JEM component in the target echo, and sufficiently utilize the information within or between the two components to extract the discriminative features for the three kinds of aircrafts. In addition, because the noise level of a test sample is usually different from those of the training samples in the real application, a simple and efficient preprocessing method is proposed for the classification stage to denoise the received test sample. Experimental results based on the simulated and measured data are presented, including the performance analysis for different dwell time, pulse repeat frequency (PRF) or signal-noise-ratio (SNR) cases and comparison with some related methods.**

***Index Terms*— Micro-Doppler, jet engine modulation (JEM), empirical mode decomposition (EMD), low resolution radar, radar target classification, feature extraction.**

I. Introduction

In the real applications, there are three levels of automatic target recognition (ATR) tasks, *i.e.*, target discrimination, target classification and target recognition. Discrimination means to distinguish multiple targets, *e.g.*, how many airplanes form a raid cluster; classification means to decide the target category, *e.g.*, an aircraft belongs to turbojet aircraft, prop aircraft or helicopter; recognition means to decide the detailed target model, *e.g.*, a turbojet aircraft is Mig-21 or Yak-42. The higher the ATR task level is, the more complicated database, the more detailed features and the larger computation burden are needed.

Manuscript received September 18, 2012; revised December 10, 2012 and February 17, 2013; accepted June 25, 2013. Date of publication July 3, 2013; date of current version October 4, 2013. This work was supported in part by the National Science Foundation of China under Grants 61271024, 61201296 and 61231017, and the Foundation for Author of National Excellent Doctoral Dissertation of China under Grant FANEDD-201156. The associate editor coordinating the review of this paper and approving it for publication was Dr. Kailash Thakur. (*Corresponding author: L. Du.*)

The authors are with the National Laboratory of Radar Signal Processing, Xidian University, Xi'an 710071, China (e-mail: dulan@mail.xidian.edu.cn; wbsatr@163.com; xidianlyb@163.com; hwliu@xidian.edu.cn).

Color versions of one or more of the figures in this paper are available online at http://ieeexplore.ieee.org.

Digital Object Identifier 10.1109/JSEN.2013.2272119

For most conventional air defense radar systems, which belong to low-resolution radars, since their range resolutions are much larger than the airplane targets' sizes, an aircraft is usually regarded as a "point" target. Due to the limited information contained in the low-resolution echoes, it is difficult to make the conventional low-resolution radar provide the target's model information, *i.e.*, target recognition. Therefore, in the real application, the low-resolution radar and high-resolution radar are usually alternately utilized, of which low-resolution radar is to detect targets and high-resolution radar is to recognize targets. If the low-resolution radar can make an initial categorization of the detection, *i.e.*, target classification, it will be much easier for the high-resolution radar to recognize the target model, *i.e.*, target recognition, based on the target classification results, since the template database to be matched can be reduced. Thus finding practical classification methods for low-resolution radar is an important research subject in radar automatic target recognition (RATR) area.

When radar illuminates a moving target, the carrier frequency of the returned signal will be shifted. This phenomenon is known as Doppler effect. If the target or any structural component of the target has oscillatory or rotation motion, which is referred to as micro-motion, such micro-motion may induce the additional Doppler modulation that generates sideband frequencies around the target's Doppler frequency, which is called as micro-Doppler effect. Chen *et al.* introduced the notion of micro-Doppler to radar area, and analyzed some kinds of micro-Doppler modulations with mathematical models [10], [11]. Different kinds of targets may have different kinds of micro-motions, thereby the discriminative features for identifying radar targets may be extracted from the corresponding micro-Doppler modulations. Lots of researches on the applications of micro-Doppler effects have been presented in radar area [1], [6], [9], [16], [19], [22], [23], [26], [28], [29], [33], [34], [36], [37], [39], [44]. The micro-Doppler signatures of different micro-motions for low resolution radar system are analyzed in [5], [6], [9], [16], [29], [39]. Papers [1], [18], [44] investigate the ISAR imaging of a target with micro-motion, and papers [22], [31], [36], [37] analyze the micro-Doppler effect in ISAR/SAR image. Extraction and classification of micro-Doppler feature for pedestrians and vehicles are discussed in [3], [19], [25], [26], [28], [33]–[35], which demonstrate that micro-Doppler signatures and the corresponding micro-Doppler features can be utilized for classification of targets with different micro-motions.

The jet engine modulation (JEM) characteristic, *i.e.*, the periodical modulated echo produced by the high-speed rotating structures (rotating wings, fans or props) in an aircraft, is a kind of micro-Doppler effects for airplane targets. JEM induces that the Doppler spectrum is uniformly located as line spectrum on both sides of the carrier frequency, and the interval between the modulated spectrum lines is determined by the number of blades and their rotation speeds [2]. Most existing methods of extracting JEM features estimate the periodicity of modulated wave and the interval between the modulated spectrum lines [14], [24], [27], [39]. However, similar to some existing micro-Doppler feature extraction methods, these JEM parameter estimation methods generally require sufficiently high pulse repeat frequency (PRF) or sufficiently long dwell time to achieve good performance, thus it is difficult for a surveillance radar to accomplish the task of simultaneous detection and classification via such methods. Recent paper [8] proposes to use the eigenvalue spectrum of the modulated target echo in time domain to extract low-dimensional JEM feature vector, which can describe the differences in the numbers of Doppler spectrum lines between the three kinds of aircrafts, *i.e.*, turbojet aircraft, prop aircraft and helicopter, and the inspiring classification performance is achieved with the relatively low PRF and the relatively short dwell time based on the simulated data. Nevertheless, for an airplane target, since the energy of the fuselage component is large relative to that of the JEM component in the returned echo, the fuselage component is in the dominant position in the eigenvalue spectrum and the detailed structure of the JEM component cannot be well described via the eigenvalue spectrum, which restricts the classification capability of the features extracted from the eigenvalue spectrum.

The research reported here seeks an alternative approach to distinguish the three kinds of aircrafts not only with the relatively low PRF and the relatively short dwell time but also under a relatively low Signal-Noise-Ratio (SNR) condition, which can well describe the detailed structure of the JEM component and reduce the receiver noise effects for the classification as well. The main characteristic of the proposed model can be summarized as follows:

- *A 2-step feature extraction method is developed based on EMD algorithm and CLEAN technique to decompose the fuselage component, the JEM component and the ground clutter component in the time domain signal from an aircraft.* Unlike Fourier transform and wavelet transform which map the signal space onto a space spanned by a predefined basis. Empirical Mode Decomposition (EMD) is an adaptive analysis tool that decomposes a given signal into a number of "basis functions" termed Intrinsic Mode Functions (IMFs), which are derived directly from the signal. Since EMD was first proposed by Huang *et al.* [17] in 1998, it has been widely studied by many scholars in theory [15], [30], [38], [42], [43], and in application of radar [1], [5], [6]. CLEAN is a classical signal deconvolution technique originally for improving the quality of microwave imaging [40] that can successively remove the large harmonic components from a signal. Papers [1], [5], [6] showed that EMD can separate the bulk or fuselage component and the micro-motion or JEM component in radar signals from a moving vehicle or an aircraft for further analysis on the micro-Doppler signature or ISAR imaging of the micro-motion target. Nevertheless, the experiments in [1] only process a small set of data from An-26. Our experiments based on measured data of many airplane targets from all of the three kinds (*i.e.*, turbojet aircraft, prop aircraft and helicopter) show that some returned echo from a prop aircraft cannot be decomposed into one IMF corresponding to the fuselage component and another IMF corresponding to the JEM component only via EMD. In this paper, EMD algorithm first decomposes the returned echo of an aircraft into IMFs for ground clutter suppression and feature extraction, then CLEAN technique separates the fuselage component and the JEM component for further feature extraction.
- *A low-dimensional feature vector is extracted within or between the components decomposed via EMD and CLEAN methods.* After making an analysis on the decomposition results of the measured data via EMD and CLEAN, we find differences in the IMFs of a given level, the JEM components and the fuselage components between the three kinds of aircrafts, and propose a five-dimensional feature vector to describe such discriminative information.
- *A simple and efficient preprocessing method is proposed for the classification stage to denoise the received test sample.* According to the experimental results in [8], the classification performance usually descends with the reduction of Signal-Noise-Ratio (SNR), and dramatically deteriorates especially in the low SNR case. Since the SNR directly relates to the distance between the target and radar for a given noise power and radar power, noise robustness of a classification method is an important factor in increasing the classification distance between the target and radar in the real application. Inspired by the recent work on sparse representation for noise reduction [7], [12], we develop a simpler and more efficient noise reduction method based on the noise level prior.

The reminder of the paper is organized as follows. A brief review of the micro-motion model of the rotating structures in an airplane target is provided in Section II. We make an analysis on the measured data from the three kinds of aircrafts via EMD and CLEAN methods in Section III and introduce the robust classification scheme in Section IV. The classification results and corresponding analysis based on the simulated and measured data are given in Section V, followed by the conclusion in Section VI.

II. Review of Micro-Motion Model of Rotating Structures in an Aircraft

A. Theoretical Model

According to [2], the theoretical returned signal from the rotating structures in an aircraft with the low-resolution radar

TABLE I
ROTATION SPEEDS AND CONFIGURATION PARAMETERS OF THE ROTATING STRUCTURES OF 6 TURBOJETS (T), 9 PROP AIRCRAFTS (P) AND 10 HELICOPTERS (H)

Aircraft index	Rotate speed f_r (r/s)	L_1 (m)	L_2 (m)	Blade number n	Aircraft index	Rotate speed f_r (r/s)	L_1 (m)	L_2 (m)	Blade number n
T-1	40.0	0.30	1.00	30	P-8	29.8	0.40	1.42	3
T-2	68.0	0.20	0.60	33	P-9	44.9	0.30	0.85	2
T-3	45.0	0.30	0.90	50	H-1	5.90	0	7.32	2
T-4	37.0	0.38	1.10	38	H-2	5.30	0	8.18	4
T-5	43.4	0.28	0.90	33	H-3	9.60	0	4.70	5
T-6	51.0	0.24	0.80	30	H-4	5.40	0	7.90	4
P-1	14.6	0.97	2.87	4	H-5	5.90	0	7.31	2
P-2	21.9	0.51	1.856	3	H-6	5.80	0	7.30	4
P-3	25.5	0.44	1.636	3	H-7	3.90	0	12.04	7
P-4	31.5	0.34	1.33	2	H-8	7.40	0	5.50	4
P-5	46.9	0.25	0.85	2	H-9	6.00	0	7.335	4
P-6	31.5	0.372	1.30	3	H-10	5.40	0	7.80	4

system is given by

$$x_{\mathrm{JEM}}(t) = \exp(-j2\pi f_d t)\sum_{m=0}^{N-1}(L_{2m}-L_{1m}) \sum_{k=0}^{n_m-1}[G_{1m}+G_{2m}\sin(\theta_{k,m}+\omega_{rm}t-\alpha)] \cdot\mathrm{sinc}\left(\frac{2\pi}{\lambda}(L_{2m}-L_{1m})\cos(\beta')\cos(\theta_{k,m}+\omega_{rm}t-\alpha)\right) \cdot\exp\left\{-j\frac{4\pi}{\lambda}\left[R_0+\frac{(L_{1m}+L_{2m})}{2}\cos(\beta')\right]\cos(\theta_{k,m}+\omega_{rm}t-\alpha)\right\} \quad (1)$$

where N denotes the number of rotating structures in the aircraft, L_{1m} denotes the distance of the blade roots from the center of rotation in the $(m+1)$th rotating structure, L_{2m} denotes the distance of the blade tips from the center of rotation in the $(m+1)$th rotating structure, n_m denotes the number of blades in the $(m+1)$th rotating structure, ω_{rm} denotes the rotation radian frequency of the $(m+1)$th rotating structure, R_0 denotes the range of the center of rotation to radar, and λ denotes the radar wavelength. The fuselage Doppler frequency $f_d = \frac{2v}{\lambda}$, where v denotes the radial velocity of the fuselage with respect to radar. The two terms $G_{1m} = \sin(|\beta'|+\vartheta_m)+\sin(|\beta'|-\vartheta_m)$ and $G_{2m} = \mathrm{sign}(\beta')[\sin(|\beta'|+\vartheta_m)-\sin(|\beta'|-\vartheta_m)]$ depend on the modulation produced by the blades' twist angle of the $(m+1)$th rotating structure, denoted via ϑ_m. The initial rotation angle of the $(k+1)$th blade in the $(m+1)$th rotating structure is $\theta_{k,m} = \theta_{0,m}+\frac{2\pi k}{n_m}$ with $k = 0, 1, \cdots, N_m-1$ and $m = 0, 1, \cdots, N-1$. α and β respectively represent the azimuth angle and the pitching angle between the plane of rotation and the radar line-of-sight (LOS), which is from the radar to the center of rotation. In (1), when the plane of rotation is parallel to the airplane's flying direction, $\beta' = \beta$; when they are vertical, $\beta' = \frac{\pi}{2}-\beta$.

By applying Fourier transformation on (1), the ideal JEM Doppler spectrum is as follows [2]:

$$X_{\mathrm{JEM}}(f) = \sum_{m=0}^{N-1}\sum_{i=-N_{1m}}^{N_{1m}} c_{m,i}\,\delta(f-f_d+iq_m n_m f_{rm}) \quad (2)$$

where $\delta(\cdot)$ represents the unit impulse function, $f_{rm} = \frac{\omega_{rm}}{2\pi}$ represents the rotation cyclic frequency of the $(m+1)$th rotating structure, $q_m = 1$ for even blades and $q_m = 2$ for odd blades. (2) describes a frequency modulated signal with N_{1m} pairs of spectrum lines about the center frequency of the target, each separated by $f_{Tm} = q_m n_m f_{rm}$. The amplitude of each spectrum line $c_{m,i}$ is determined by parameters λ, L_{1m}, L_{2m}, β', N_m, $\theta_{0,m}$ and Bessel function [2]. The number of spectrum lines N_{1m} is [2]

$$N_{1m} = \frac{8\pi(L_{2m}-L_{1m})\cos(\beta')}{q_m n_m \lambda} \quad (3)$$

Table I lists the rotation speeds and configuration parameters of the rotating structures of 6 turbojets, 9 prop aircrafts and helicopter. As shown in Table I, the number of blades, n_m, of a turbojet aircraft is much more than that of a prop aircraft or a helicopter, while a prop aircraft and a helicopter usually have the approximately equivalent blades, *i.e.*, their n_ms are approximately equivalent; the rotation speed of the blades, f_{rm}, of a turbojet aircraft is commonly faster than that of a prop aircraft, and that of a prop aircraft is commonly faster than that of a helicopter; and the lengths of the blades, $L_{2m}-L_{1m}$, of the three kinds of aircrafts are also different, *i.e.*, the blades of a turbojet aircraft are usually shorter than those of a prop aircraft, and those of a prop aircraft are much shorter than those of a helicopter. Then according to (2) and (3), given the same β', the JEM Doppler spectra of the three kinds of airplanes are very discriminant, *i.e.*, the interval between the neighbouring spectrum lines, f_{Tm}, corresponding to the spectrum of a turbojet aircraft is much larger than that of a prop aircraft, and the number of spectrum lines, N_{1m}, corresponding to the spectrum of a turbojet aircraft is much

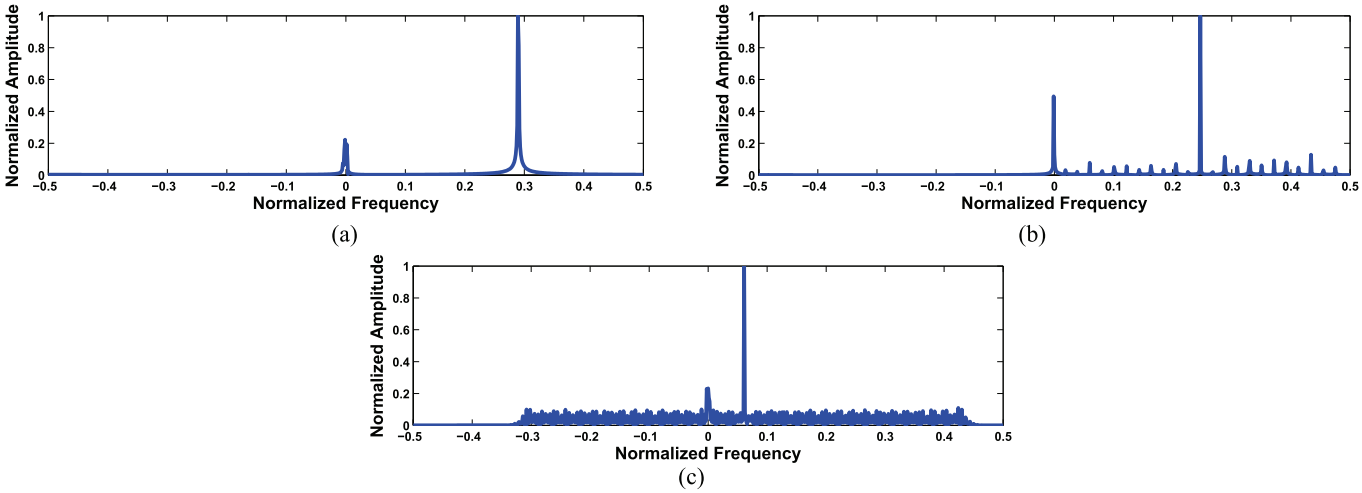

Fig. 1. Doppler spectra of the simulated data. (a) Turbojet aircraft. (b) Prop aircraft. (c) Helicopter.

fewer than that of a prop aircraft; while f_{Tm} corresponding to the spectrum of a prop aircraft is commonly larger than that of a helicopter, and N_{1m} corresponding to the spectrum of a prop aircraft is much fewer than that of a helicopter. In addition, since the rotor blades of a turbojet aircraft are installed in the turbine duct which may shield the blades for some target-aspects, sometimes the JEM component of a turbojet aircraft is too weak to be visible.

B. Analysis on Simulated Data

In the above analysis, we don't consider the fuselage component. In the real application, the fuselage RCS is much larger than that of the rotating structures. Within the several tens of milliseconds of dwell time, an airplane target can be regarded as a point traveling at a uniform velocity, thus the fuselage component echoes can be written as

$$x_{\mathrm{F}}(t) = c_{\mathrm{F}} \exp(j2\pi f_d t) \tag{4}$$

In our simulation, we assume the amplitude of the fuselage component c_{F} within the dwell time is constant, and all c_{F} of different samples from a kind of airplane targets are independently Rayleigh distributed according to Swerling fluctuation model I.

In the real application, the target area and the clutter area are mixed in the returned echo due to the range ambiguousness, therefore, we should also consider the effect of ground clutter. For the air defense radar systems considered here, the Doppler spectrum of ground clutter component mainly corresponds to the frequency components around $f = 0$. In our simulation, we use some single frequency signal around $f = 0$ to simulate the ground clutter component.

Figure 1 shows the simulated spectra of the rotating blades of the three kinds of aircrafts with the fuselage components and ground clutter. From Figure 1, we can observe that the number of spectrum lines of a helicopter is largest and its spectrum lines are densest, while a turbojet aircraft has the fewest spectrum lines and its spectrum lines are sparsest. For a prop aircraft, the number of spectrum lines and their distribution are the compromises between those of a turbojet aircraft and a helicopter.

Furthermore, comparing Figure 1 with the Doppler spectra of the measured data shown in Figure 2 in Section III-B, we can see that our simulation data of the three kinds of aircrafts are in accordance with the measured data.

III. Empirical Mode Decomposition Method and CLEAN Technique With Applications on Airplane Data Analysis

A. Empirical Mode Decomposition Method

In 1998, Huang *et al.* [17] introduced the Empirical Mode Decomposition (EMD) method for nonlinear and nonstationary signal analysis. Being quite different from Fourier transform and wavelet transform, which map the signal space onto a space spanned by a predefined basis, the general idea of EMD is the *sifting process* to decompose a given signal into a number of "basis functions" which are derived directly from the signal. These adaptive basis functions are called Intrinsic Mode Functions (IMFs). An IMF satisfies two conditions: 1) in the whole data set, the number of extrema and the number of zero-crossings must either equal or differ, at most, by one; 2) at any point, the mean value of the envelope defined by the local maxima and the envelope defined by the local minima is zero. Given a signal $\boldsymbol{x}$, the first IMF can be obtained via the sifting process described in Algorithm 1. In [17], when the change in $\boldsymbol{r}$ is negligibly small (*e.g.*, the variation rate between two iterations lower than a preset threshold), Algorithm 1 stops. In the Matlab code from [30], a fixed number of iterations (*e.g.*, 10 iterations) for each IMF component is used as the stopping criterion. In the following experiments, we use the second stopping criterion.

Once the first IMF is obtained, we store the residual $\boldsymbol{res}_1 = \boldsymbol{x} - \boldsymbol{r}$ as a new signal, and the next IMF can be obtained by applying the sifting process to the residual $\boldsymbol{res}_1$. In the same way, the remaining IMFs can be calculated and EMD ends up

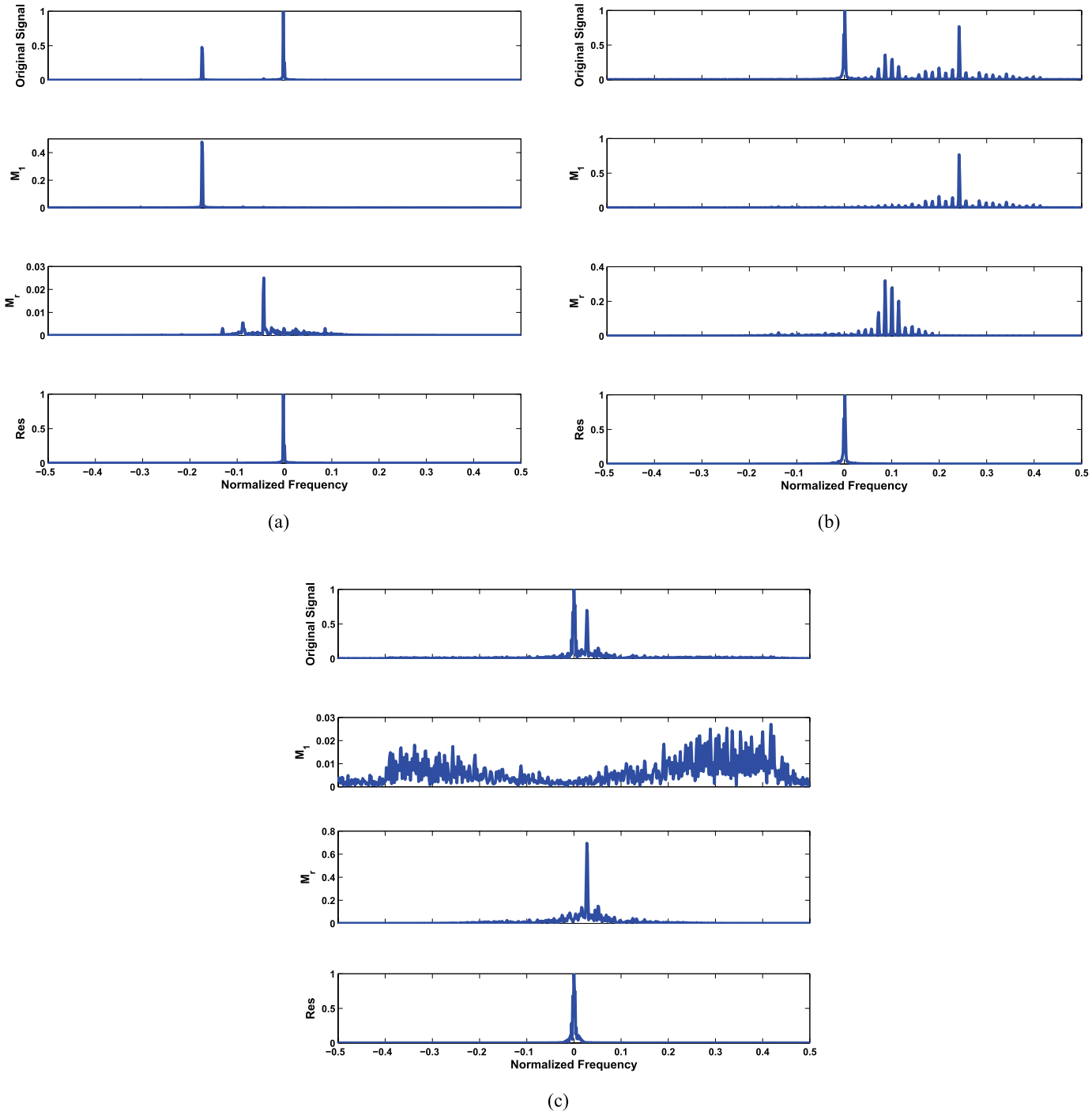

Fig. 2. Doppler spectra of the original signal, IMFs and residual component from the measured data (a) Turbojet aircraft. (b) Prop aircraft. (c) Helicopter. In each subfigure, the first row is the Doppler spectrum of the original signal, the second row is $\boldsymbol{M}_1$, the third row is $\boldsymbol{M}_r$ and the last row is the Doppler spectrum of the residual component.

with a representation of the form:

$$\boldsymbol{x} = \sum_{i=1}^{L} \boldsymbol{imf}_i + \boldsymbol{res}_L \tag{5}$$

where $\boldsymbol{imf}_i$ denotes the ith IMF component and $\boldsymbol{res}_L$ is the residual after the Lth level of decomposition. For a given signal $\boldsymbol{x}$, the maximum decomposition level L is adaptively determined via a decomposition stopping criterion. When $N_{\max}^{(L+1)} + N_{\min}^{(L+1)} < 3$ with $N_{\max}^{(L+1)}$ denoting the number of the local maxima of $\boldsymbol{res}_L$ and $N_{\min}^{(L+1)}$ denoting the number of the local minima of $\boldsymbol{res}_L$, the decomposition stops at this level [30]. Thus we get L IMFs $\{\boldsymbol{imf}_i\}_{i=1}^{L}$ and the residual $\boldsymbol{res}_L$ for the signal $\boldsymbol{x}$.

The original EMD can only be applied to real-valued signal. In most engineering environments, the quadrature-sampling technique is utilized in the receiver, and complex-valued signals with amplitude and phase information are

generated. In [30], Rilling *et al.* proposed an approach to extend EMD from real-value case to complex-value case. The main idea of this approach is that it considers the real-valued signal as the scale of its local oscillations in the 2-D plane, which means fast oscillations superimpose on slow oscillations, and the complex-valued signal as the scale of its local rotations in the 3-D space, which, similar to the real-valued case, means fast rotations superimpose on slow rotations. Then the difference between real-value EMD and complex-value EMD is that the real-value EMD attempts to extract zero-mean oscillation components while the complex-value EMD extract zero-mean rotating components. The mean processing for the complex-value "envelope", *i.e.*, 3-D envelope, is defined in [30] for the complex-value EMD. Therefore, the result of the complex-value EMD is a number of complex-value IMFs, whose rotation vector varies from fast to slow.

To understand the behavior of EMD as a decomposition procedure, Flandrin *et al.* [15] show that EMD acts essentially as a filter bank similar to those involved in wavelet decompositions. In this view, the filter associated to $\boldsymbol{imf}_1$ is essentially high-pass, and $\{\boldsymbol{imf}_i\}_{i=2}^{L}$ are characterized by a set of overlapping bandpass filters. The $\boldsymbol{imf}_1$ component occupies a frequency domain which is roughly the upper halfband of that of the original signal, and the other mode with level index $i+1$ ($i \geq 1$), $\boldsymbol{imf}_{i+1}$, occupies a frequency domain which is roughly the upper halfband of that of the previous residual with level index i ($i \geq 1$), $\boldsymbol{res}_i$. Therefore, as the level index i increases, the frequencies corresponding to the passband of $\boldsymbol{imf}_i$ will decrease. It is worth to emphasize the fact that the IMFs correspond to the automatic filters adaptive to the signal rather than the predetermined subband filters. In other words, EMD can adaptively decompose a signal into some different frequency components without predetermined bases.

B. Airplane Data Analysis Via Empirical Mode Decomposition

After applying EMD to an aircraft echo, we can get the decomposition results as (5). Define $\boldsymbol{M}_1$ and $\boldsymbol{M}_r$ as follows:

$$\boldsymbol{M}_1 = |\mathrm{FFT}(\boldsymbol{imf}_1)| \tag{6}$$

$$\boldsymbol{M}_r = |\mathrm{FFT}(\sum_{i=2}^{L} \boldsymbol{imf}_i)| \tag{7}$$

where the function $\mathrm{FFT}(\cdot)$ denotes the fast Fourier transformation (FFT).

The Doppler spectra of the original signal, IMFs and residual for the measured data of the turbojet aircraft, prop aircraft and helicopter are shown in Figure 2. From Figure 2(a) and (c), we can see that the EMD method can separate the JEM component from the fuselage component for both turbojet aircraft and helicopter effectively. Since the flight speed of a turbojet aircraft is much higher than that of a helicopter, the fuselage component of the turbojet aircraft can be regarded as a high-frequency component and that of helicopter as a low-frequency component when the PRF is relatively high. After applying EMD to the returns of a turbojet aircraft, $\boldsymbol{M}_1$ captures the high-frequency fuselage component, and the JEM component is contained in $\boldsymbol{M}_r$. On the contrary, for a helicopter, $\boldsymbol{M}_r$ mainly captures the low-frequency fuselage component, and $\boldsymbol{M}_1$ contains the JEM component. Since the spectra properties of a prop aircraft are in the compromising position between those of a turbojet aircraft and a helicopter, the decomposition results of a prop aircraft are also in the compromising position between those of the other two kinds of aircrafts. As shown in Figure 2(b), for the prop aircraft, the EMD method fails to separate the fuselage and JEM components into the different IMFs, *i.e.*, $\boldsymbol{M}_1$ contains the fuselage component and a part of the JEM component, and $\boldsymbol{M}_r$ contains the rest of the JEM component. In addition, as stated in Section III-A, EMD acts essentially as a filter bank. In this view, the $\boldsymbol{imf}_1$ component occupies a frequency domain which is roughly the upper halfband of that of the original signal, and the $\boldsymbol{imf}_{i+1}$ component with $i \geq 1$ occupies a frequency domain which is roughly the upper halfband of that of the previous residual $\boldsymbol{res}_i$ with $i \geq 1$. Therefore, if only few components are nonzero in the upper halfband frequency domain, the corresponding IMF spectrum approximately locates at a single Doppler bin; if the most components within a Doppler band are nonzero in the upper halfband frequency domain, the corresponding IMF spectrum spreads within the Doppler band. As shown in Figure 2, the $\boldsymbol{M}_1$ in Figure 2(a) locates at a single Doppler bin; while the $\boldsymbol{M}_1$ in Figure 2(b) or (c) spreads within a Doppler band.

Furthermore, Figure 2 shows that, for the three kinds of aircrafts, the ground clutter with the clutter spectrum located at the zero Doppler bin is always captured by the residual component, therefore, the clutter suppression can be achieved by just discarding the residual component without any extra processing under this condition. It is another advantage of the EMD method in this application. For some nonstationary clutter, such as sea clutter and cloud clutter, with the clutter spectrum spread within a Doppler band, according to the filter bank viewpoint, if the clutter spectrum is exactly located in the upper halfband frequency domain corresponding to an IMF component and the target signal is contained within other IMFs and the residual component, such clutter can be depressed via the removal of the corresponding IMF from the original signal. Nevertheless, in such case, the prior information about the clutter spectrum may be needed to determine that which IMF contains the clutter.

C. CLEAN Technique

According to the EMD results on the measured airplane data in Section III-B, both $\boldsymbol{M}_1$ and $\boldsymbol{M}_r$ of the example echo from a prop aircraft contain the JEM component, which means the fuselage component and the JEM component are not be decomposed into different IMFs via EMD. In order to further extract features from the fuselage component and the JEM component, we use CLEAN technique to separate the fuselage component and the JEM component from the ground clutter suppressed echo obtained via EMD.

Algorithm 1: Sifting process to obtain the first IMF

Input: $\boldsymbol{x}$

Initialization: Let $\boldsymbol{r} = \boldsymbol{x}$.

Step 1: Identify the local maxima of $\boldsymbol{r}$, and interpolate between local maxima to construct an upper envelope $\boldsymbol{r}_{\max}$.

Step 2: Identify the local minima of $\boldsymbol{r}$, and interpolate between local minima to construct a lower envelope $\boldsymbol{r}_{\min}$

Step 3: Compute the mean values of upper and lower envelopes as $\boldsymbol{m} = \frac{\boldsymbol{r}_{\max}+\boldsymbol{r}_{\min}}{2}$.

Step 4: Let $\boldsymbol{r} = \boldsymbol{r} - \boldsymbol{m}$.

Step 5: If a stopping criterion is met, designate this $\boldsymbol{r}$ as $\boldsymbol{imf}_1$. Otherwise, repeatedly apply Steps 1-4 to $\boldsymbol{r}$, until the stopping criterion is met.

Since the residual $\boldsymbol{r}_L$ obtained via EMD corresponds to the ground clutter component if it exists, the clutter suppressed echo can be reconstructed as

$$\tilde{\boldsymbol{x}} = \sum_{i=1}^{L} \boldsymbol{imf}_i \tag{8}$$

According to (2), the returned echo from the rotating structures in an aircraft are the summation of several series of equal interval harmonic waves [8]. As discussed in Section II-B, the returned echo from the fuselage component can be considered as a single frequency signal corresponding to its Doppler frequency f_d, *i.e.*, (4). Therefore, the radar returned echoes with fuselage component can still be described as the summation of harmonic wave models.

$$\tilde{x}(t) = \sum_{n=1}^{K} \rho_n \exp[j(2\pi f_n t + \phi_n)] \tag{9}$$

where K denotes the total number of harmonic waves. CLEAN is a classical signal deconvolution technique that can successively remove the large harmonic components from a signal [40]. Since the fuselage component is much larger than the JEM component for an airplane target, the largest harmonic wave in (9) corresponds to the fuselage component and the rest harmonic waves correspond to the JEM component. Therefore, by applying CLEAN algorithm to $\tilde{\boldsymbol{x}}$ once, we can separate the fuselage component and the JEM component. The detailed procedure is presented in Algorithm 2.

The CLEAN technique can also be utilized for the ground clutter suppression [33]. The main difference between EMD and CLEAN methods for the ground clutter suppression is that the EMD method can adaptively remove the ground clutter component from a given signal; while the CLEAN technique needs to preset a proper bandwidth value for the ground clutter in the given signal before removing it, and the different settings of the bandwidth may affect its clutter suppression performance [33].

D. Airplane Data Analysis Via CLEAN

After applying CLEAN to the clutter suppressed echo from an aircraft, we can separate the fuselage component $\boldsymbol{x}_{\mathrm{F}}$ and the JEM component $\boldsymbol{x}_{\mathrm{JEM}}$ as shown in Algorithm 2. We use $\boldsymbol{X}_{\mathrm{F}}$ and $\boldsymbol{X}_{\mathrm{JEM}}$ to represent the Fourier transformations of $\boldsymbol{x}_{\mathrm{F}}$ and $\boldsymbol{x}_{\mathrm{JEM}}$.

Figure 3 shows the CLEAN results of the clutter suppressed measured data from the turbojet aircraft, prop aircraft and helicopter respectively. As shown in Figure 3, the fuselage and JEM components can be effectively separated by applying the CLEAN technique. Since the measured data used in Figure 3 are same as those in Figure 2, compared with the EMD results in Figure 2 (especially for (a) and (c)), we can see that the detailed structure of the JEM component of the turbojet aircraft can be better described via the CLEAN technique, and the JEM component of the helicopter can be separated more clearly from its fuselage component via the CLEAN technique.

IV. Robust Classification Scheme

A. Noise Reduction Approach

In the above analysis, we only consider the fuselage component, the JEM component and the ground clutter component contained in the airplane target echo. In the real application, the returned echo also contains the noise component.

In (9), $\tilde{x}(t)$ represents the clutter suppressed echo. According to Figure 2, the ground clutter component can also be represented by the harmonic waves around $f = 0$. Thus the returned echo of an aircraft with the fuselage component, the JEM component, the ground clutter component and the noise component can be represented as

$$x(t) = \sum_{n=1}^{K} \rho_n \exp[j(2\pi f_n t + \phi_n)] + w(t) \tag{10}$$

where $w(t)$ represents the noise component. According to (10), the returned signals of the fuselage component, the JEM component and the ground clutter component can be represented by Fourier series; while the noises in the inphase and quadrature echoes of a target can be assumed to be Gaussian white noise with zero mean and covariance $\sigma^2/2$ for aircraft-like targets under a look-up scenario such as the case considered in this paper. Then

$$\boldsymbol{x} = \boldsymbol{B}\boldsymbol{a} + \boldsymbol{w} \tag{11}$$

where $\boldsymbol{B}$ is the Fourier basis matrix, and $\boldsymbol{a}$ represents the corresponding coefficients. The general entry of the $T \times M$ basis matrix $\boldsymbol{B}$ is

$$B(t, f) = \exp(j\frac{2\pi t}{T} f), t = 0, 1, \cdots, T-1, \quad f = 0, 1, \cdots, M-1 \tag{12}$$

where T is the length of the signal $\tilde{\boldsymbol{x}}$ and M denotes the length of the Doppler spectrum. When $T = M$, $\boldsymbol{B}$ is a complete orthogonal basis matrix, and the solution of $\boldsymbol{a}$ is unique; when $T < M$, $\boldsymbol{B}$ is redundant basis matrix, and the super-resolution representation can be achieved via some optimization method

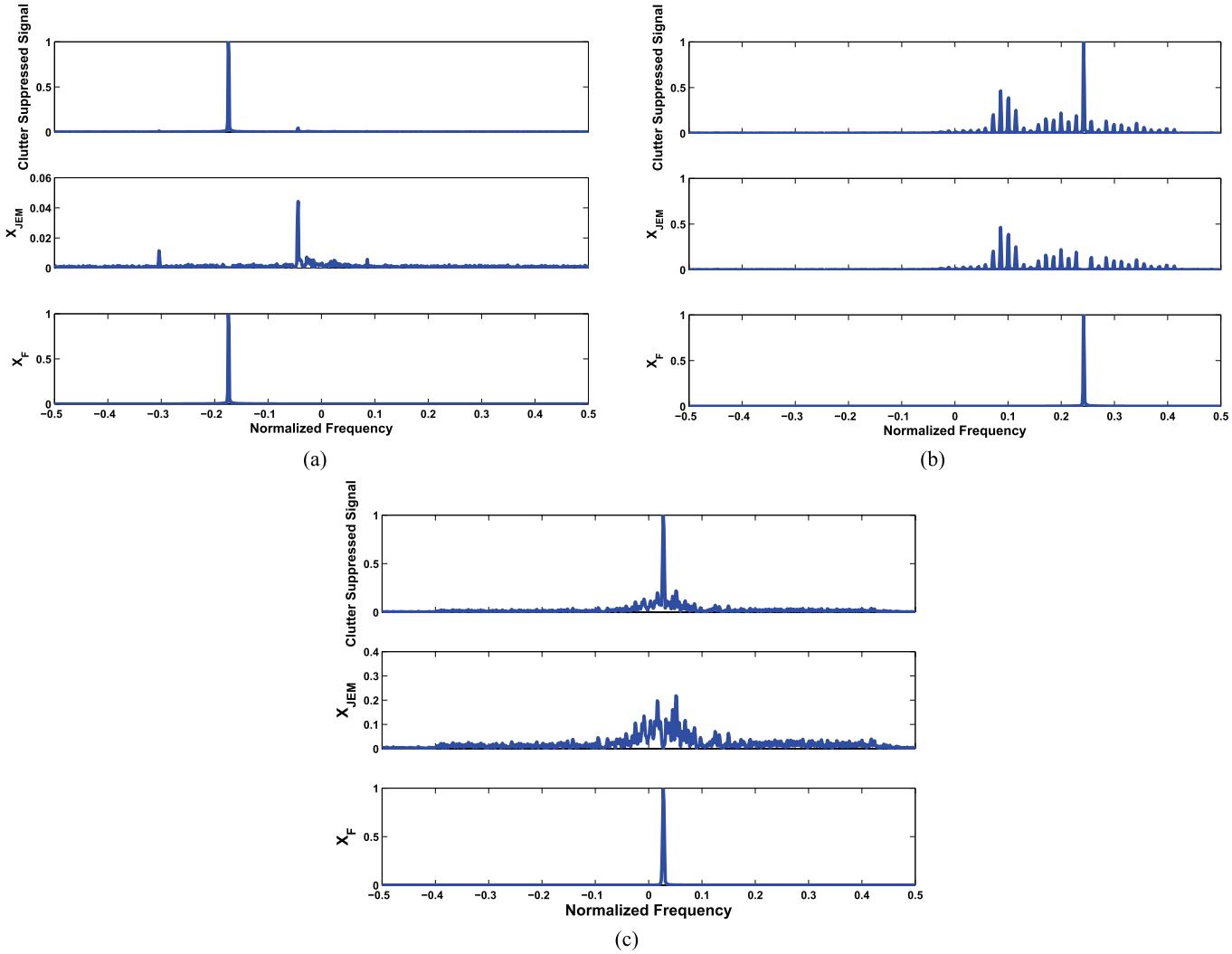

Fig. 3. CLEAN results of the clutter suppressed signal from the measured data. (a) Turbojet aircraft. (b) Prop aircraft. (c) Helicopter. In each subfigure, the first row is the Doppler spectrum of the clutter suppressed signal, the second row is $\boldsymbol{X}_{\mathrm{JEM}}$ and the third row is $\boldsymbol{X}_{\mathrm{F}}$. The measured data used here are same as those in Figure 2.

Algorithm 2: CLEAN algorithm to separate the fuselage component and the JEM component in the clutter suppressed echo

Input: $\tilde{\boldsymbol{x}}$

Step 1: Calculate $\tilde{\boldsymbol{X}} = \mathrm{FFT}(\tilde{\boldsymbol{x}})$.

Step 2: Find the maxima point in $\tilde{\boldsymbol{X}}$, calculate the corresponding Doppler frequency f_1 based on the position of the maxima point, and record the corresponding amplitude ρ_1 and phase ϕ_1.

Step 3: Reconstruct the largest harmonic wave as $x_{\mathrm{F}}(t) = \frac{\rho_1}{T}\exp[j(2\pi f_1 t + \phi_1)]$ with $t = 1, 2, \cdots, T$.

Step 4: Subtract, that is, CLEAN, the contribution of the detected frequency component as a harmonic wave from the echo data: $\boldsymbol{x}_{\mathrm{JEM}} = \tilde{\boldsymbol{x}} - \boldsymbol{x}_{\mathrm{F}}$.

Step 5: $\boldsymbol{x}_{\mathrm{F}}$ is the fuselage component and $\boldsymbol{x}_{\mathrm{JEM}}$ is the JEM component.

used in sparse reconstruction or compressed sensing (CS) [7], [12]. Due to the algorithm complexity and the large computation burden for the case $T < M$, here we only consider the case $T = M$, for which the coefficients $\boldsymbol{a}$ can be easily obtained via orthogonal projection.

From (11),

$$\|\boldsymbol{x} - \boldsymbol{B}\boldsymbol{a}\|_2 = \|\boldsymbol{w}\|_2 \tag{13}$$

where $\|\cdot\|_2$ denotes the l_2 norm of a vector, $\|\boldsymbol{w}\|_2 = \sqrt{N}\sigma$. Therefore, noise reduction can be achieved via imposing the small coefficients $\hat{\boldsymbol{a}}_f$ to be zero with the reconstruction error $\|\boldsymbol{x} - \boldsymbol{B}\hat{\boldsymbol{a}}\|_2 \leq \epsilon$, where ϵ is associated with the noise level σ. The noise considered here mainly refers to the heat noise from the receiver, which can be assumed to be stationary, accordingly, there are several ways to accurately estimate the noise power (*i.e.*, noise variance σ^2) [32], of which a simple approach is to measure the noise power from the receiver with no input signal. This noise reduction method is inspired by the sparse representation work for noise reduction, but it is much simpler and more efficient than the sparse representation methods.

Most existing classification methods assume that the training data and test data are obtained under the similar measurement circumstance. In the real application, the training

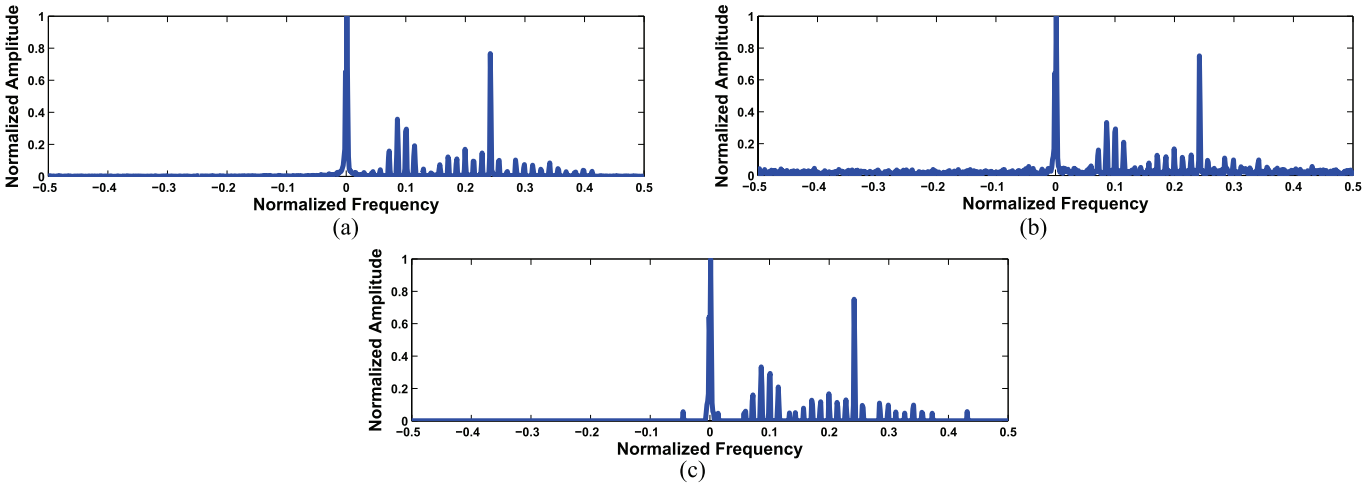

Fig. 4. The Doppler spectra of the measured data for a prop aircraft. The measured data used here is same as that in Figure 2(b). (a) The Doppler spectrum of the original signal under the high SNR condition, which is same as the first row in Figure 2(b). (b) The Doppler spectrum of the noised signal under the SNR condition of 10 dB. (c) The Doppler spectrum of the denoised signal via the proposed noise reduction approach.

data are usually collected under the condition of high SNR via some cooperative measurement experiments or directly via simulations as our following experiments; while the test samples are usually got in the non-cooperative circumstance (e.g., at the battle time), where the high SNR cannot be guaranteed due to the severe measurement conditions, such as the large distance between the non-cooperative targets and radar. Therefore, we will use the noise reduction method introduced above as a preprocessing method in the classification stage in our classification scheme to improve its noise robustness and further increase the classification distance between the target and radar in the real application.

Figure 4 gives a noise reduction example based on the measured data from a prop aircraft. The measured data used in Figure 4 is same as that in Figure 2(b). The Doppler spectra of the original signal under the high SNR condition and that under the SNR condition of 10 dB are shown in Figure 4(a) and (b). After applying the proposed noise reduction approach to the noised signal shown in Figure 4(b), we get the Doppler spectra of the denoised signal depicted in Figure 4(c). Comparing Figure 4(a), (b) and (c), we can see that the proposed noise reduction approach can effectively reduce the noise component and have little effect on the original signal.

B. EMD-CLEAN Feature Extraction

1) Features Extracted from EMD Results: As shown in Figure 2, we can find some differences in the components $\boldsymbol{M}_1$ and $\boldsymbol{M}_r$ between the three kinds of airplane targets. Here we use the following two features to depict the distinctions:

- Feature 1: $\mathcal{F}_{\mathrm{EMD}}(1) = \mathrm{entropy}(\boldsymbol{M}_1) = -\sum_{f=1}^{T} p_f \log(p_f)$ with $p_f = M_1^2(f)/(\sum_{f=1}^{T} M_1^2(f))$ and $\boldsymbol{M}_1 = \{M_1(f)\}_{f=1}^{T}$, which represents the energy entropy of $\boldsymbol{M}_1$. The defined energy entropy indicates the energy distribution of a series, the more the energy gathers, which means the more a series close to an impulse function, the less the entropy is.
- Feature 2: $\mathcal{F}_{\mathrm{EMD}}(2) = \sum_{f=1}^{T}(l - \bar{f})^2 \bar{M}_r(f)$ with $\bar{M}_r(f) = M_r(f)/(\sum_{f=1}^{T} M_r(f))$, $\bar{f} = \sum_{f=1}^{T} f \times \bar{M}_r(f)$ and $\boldsymbol{M}_r = \{M_r(f)\}_{f=1}^{T}$, which represents the 2nd order central moment of $\boldsymbol{M}_r$. The 2nd-order central moment describes the distribution of a series relative to its centroid.

2) Features Extracted from CLEAN Results: As shown in Figure 3, we can find some differences in the fuselage and JEM components between the three kinds of airplane targets. Here we use the following three features to depict the distinctions:

- Feature 1: $\mathcal{F}_{\mathrm{CLEAN}}(1) = \mathrm{entropy}(\boldsymbol{X}_{\mathrm{JEM}})$, which represents the energy entropy of the JEM spectrum $\boldsymbol{X}_{\mathrm{JEM}}$. The detailed calculation and explanation of the energy entropy is discussed in the introduction of $\mathcal{F}_{\mathrm{EMD}}(1)$ in Section IV-B.1.
- Feature 2: $\mathcal{F}_{\mathrm{CLEAN}}(2) = \sum_{f=1}^{T} X_{\mathrm{JEM}}(f)/(\max(\boldsymbol{X}_{\mathrm{JEM}}))$ with $\max(\boldsymbol{X}_{\mathrm{JEM}})$ denoting the maximum value of the JEM spectrum $\boldsymbol{X}_{\mathrm{JEM}} = \{X_{\mathrm{JEM}}(f)\}_{f=1}^{T}$, which represents the summation of the JEM spectrum normalized by the maximum element. This feature can describe the spectrum distribution of the JEM component.
- Feature 3: $\mathcal{F}_{\mathrm{CLEAN}}(3) = \|\boldsymbol{x}_{\mathrm{F}}\|_2 / \|\|\boldsymbol{x}_{\mathrm{JEM}}\|_2$, which represents the energy ratio between the fuselage component and the JEM component.

C. Classification Scheme

A typical statistical recognition scheme is depicted in Figure 5. As we can see, there are two stages, *i.e.*, training stage and classification stage, in the classification procedure.

In the training stage, we use the simulated data of the three kinds of aircrafts, where the ground clutter and receiver noise components can be ignored. Firstly, we apply EMD to each training sample, and get IMF components as discussed in Section III-A. Then the feature vector $\boldsymbol{\mathcal{F}}_{\mathrm{EMD}} = [\mathcal{F}_{\mathrm{EMD}}(1), \mathcal{F}_{\mathrm{EMD}}(2)]$ is extracted as described in Section IV-B.1. Secondly, we apply CLEAN to each training

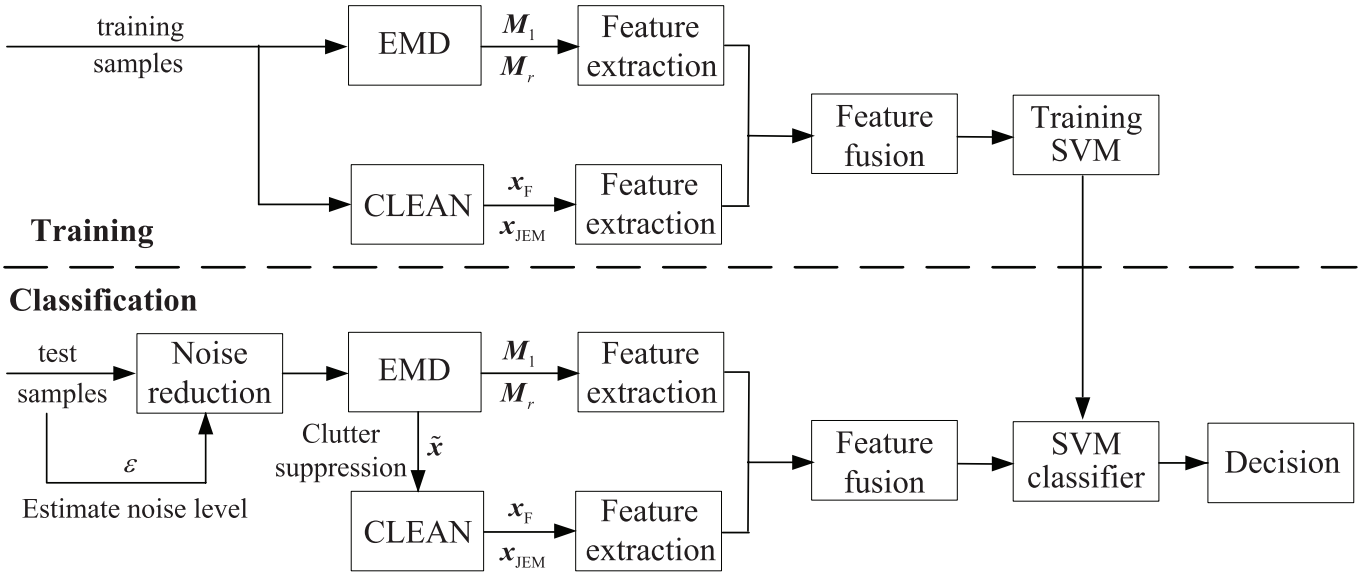

Fig. 5. A flow chart of our classification method.

sample, get the fuselage component $\boldsymbol{x}_{\mathrm{F}}$ and the JEM component $\boldsymbol{x}_{\mathrm{JEM}}$ as discussed in Section III-C. Then the feature vector $\boldsymbol{\mathcal{F}}_{\mathrm{CLEAN}} = [\mathcal{F}_{\mathrm{CLEAN}}(1), \mathcal{F}_{\mathrm{CLEAN}}(2), \mathcal{F}_{\mathrm{CLEAN}}(3)]$ is extracted as described in Section IV-B.2. Finally, the compounded feature vector $\boldsymbol{\mathcal{F}} = [\boldsymbol{\mathcal{F}}_{\mathrm{EMD}}, \boldsymbol{\mathcal{F}}_{\mathrm{CLEAN}}]$ is used to train the support vector machine (SVM) classifier. The SVM is fundamentally a two-class classifier. There is no uniform method for combining multiple two-class SVMs in order to build a multi-class classifier. Here we use the quadratic-programming based SVM (QP-SVM) proposed in [41] in the following experiments. This classifier defines a single objective function for training all one-versus-the-rest two-class SVMs simultaneously, based on maximizing the margin for each two-class SVM. Contrast to the one-versus-the-rest (OAA) [4] and one-versus-one (OAO) [20] approaches, the QP-SVM can avoid ambiguities in the resulting classification. The main disadvantage of the QP-SVM is the much slower training for a large number of categories. Nevertheless, here we only consider the three-class classification problem.

In the classification stage, we may use the simulated or measured data, which should contain the ground clutter and receiver noise components. Firstly, we use the noise reduction method introduced in Section IV-A to denoise each test sample which is measured under low SNR condition. Secondly, we apply EMD to each test sample, and get IMF components as discussed in Section III-A. Then the feature vector $\boldsymbol{\mathcal{F}}_{\mathrm{EMD}} = [\mathcal{F}_{\mathrm{EMD}}(1), \mathcal{F}_{\mathrm{EMD}}(2)]$ is extracted as described in Section IV-B.1. Thirdly, we apply CLEAN to the ground clutter suppressed sample $\tilde{\boldsymbol{x}}$, which can be reconstructed from the results of EMD, get the fuselage component $\boldsymbol{x}_{\mathrm{F}}$ and the JEM component $\boldsymbol{x}_{\mathrm{JEM}}$ as discussed in Section III-C. Then the feature vector $\boldsymbol{\mathcal{F}}_{\mathrm{CLEAN}} = [\mathcal{F}_{\mathrm{CLEAN}}(1), \mathcal{F}_{\mathrm{CLEAN}}(2), \mathcal{F}_{\mathrm{CLEAN}}(3)]$ is extracted as described in Section IV-B.2. Finally, the SVM classifier learned in the training stage is used to give the classification decision for the compounded feature vector $\boldsymbol{\mathcal{F}} = [\boldsymbol{\mathcal{F}}_{\mathrm{EMD}}, \boldsymbol{\mathcal{F}}_{\mathrm{CLEAN}}]$ of each test sample.

V. Experimental Results

Two experimental schemes are designed in this section to verify the performance of the classification scheme we proposed above. In the first experiment, we make the classification performance analysis on our proposed scheme and some related classification methods not only with the different dwell time and PRF cases but also under the different SNR cases based on the simulated data. In the second experiment, we only compare the classification performance of our scheme and the related methods under the different SNR test conditions based on the measured data, since the dwell time and PRF of the measured data are fixed.

In the following experiments, we compare our classification scheme with the three related methods which are described as follows.

- The eigenvalue spectrum method: This method is proposed in [8], which uses a four-dimensional feature vector from the eigenvalue spectrum of the aircraft target echo to discriminate the three kinds of the aircrafts. The moving-target indicator (MTI) filter with a double canceler [21] is used in this method to suppress the ground clutter before feature extraction. To compare the classification performance fairly, we also use the noise reduction approach proposed in Section IV-A as a preprocessing step for this method in the following experiment.
- The CLEAN method: In this method, the ground clutter is first suppressed by the CLEAN technique, then we extract the three-dimensional feature vector from the fuselage and JEM components separated via the CLEAN technique, which are introduced in Section IV-B.2 and denoted as $\boldsymbol{\mathcal{F}}_{\mathrm{CLEAN}} = [\mathcal{F}_{\mathrm{CLEAN}}(1), \mathcal{F}_{\mathrm{CLEAN}}(2), \mathcal{F}_{\mathrm{CLEAN}}(3)]$, to discriminate the three kinds of aircrafts. For the same reason, we also use the proposed noise reduction approach as a preprocessing step for this method in the following experiment.

- The EMD-CLEAN method without the proposed noise reduction approach: To evaluate the performance of the noise reduction approach proposed in Section IV-A, we also compare our noise-robust classification scheme proposed in Section IV-C with the non-robust one (*i.e.*, that without the noise reduction preprocessing step).

For simplicity, the classification scheme proposed in Section IV-C, the eigenvalue spectrum method with the proposed noise reduction approach, the CLEAN method with the proposed noise reduction approach and the EMD-CLEAN method without the proposed noise reduction approach are referred to as *Robust EMD-CLEAN*, *Robust EIG-SPECTRUM*, *Robust CLEAN* and *EMD-CLEAN* respectively in the following experiments.

The SVM with Gaussian kernel is chosen as the classifier in our experiments. The parameter of Gaussian kernel is tuned in the range $[0, 5]$ for each classification method, and we select the best classification result from those of the different parameter settings for the following analysis and comparison.

A. Experiment on Simulated Data

In this experimental scheme, both the training sets and the test sets are simulated based on the theoretical model introduced in Section II. Table I lists the simulation parameters of the rotating structures of the 25 aircrafts, which includes 6 turbojet aircrafts, 9 prop aircrafts and 10 helicopters. For each aircraft category, we use half of the aircraft models as the training aircraft models, from which the training data are simulated, and the rest models are used as the test aircraft models, from which the test data are simulated. We assume both the turbojet aircrafts and the prop aircrafts have two rotating fans with the same configuration and rotation speed while they differ in the initial rotation angle. For helicopters, since the echoes are mainly affected by the main rotor which is larger in size than the tail rotor. In our simulation, we simply set the length of the tail rotor is 1/4 of that of the main rotor and the corresponding rotation speed is 4 times that of the main rotor. The flight speeds of the turbojet aircraft, prop aircraft and helicopter are set within $[150\text{m/s}, 200\text{m/s}]$, $[90\text{m/s}, 150\text{m/s}]$ and $[30\text{m/s}, 70\text{m/s}]$ respectively. Besides the flight speeds, the flight altitudes and the pitching angles between the plane of rotation and the radar LOS also randomly vary within some given ranges in our simulation. Additionally, there are no ground clutter component and receiver noise component in the training data, but the test data contain these components.

The classification accuracies of Robust EMD-CLEAN, Robust EIG-SPECTRUM, Robust CLEAN and EMD-CLEAN versus the dwell time, PRF and test SNR are shown in Figure 6(a), (b) and (c) respectively. For each subfigure in Figure 6, given a set of radar or test condition parameters, there are one training set and three test sets (the flight scene parameters of the test aircraft models, including the flight speeds, the flight altitudes and the pitching angles between the plane of rotation and the radar LOS, are different between the three test sets) for all four classification methods, which are simulated as described above. The classification rates shown in Figure 6 are averaged over the three runs with the three test datasets. For Figure 6(a), the radar carrier frequency is 1.3 GHz (L band), the PRF is 4KHz and the test SNR is 15 dB. As shown in Figure 6(a), the average classification rates of all four methods increase as the dwell time increases. When the dwell time $\geq$ 20ms, our proposed Robust EMD-CLEAN method performs better than the other three methods. For Figure 6(b), the radar carrier frequency is 1.3GHz (L band), the dwell time is 30ms and the test SNR is 15 dB. As shown in Figure 6(b), when the PRF is 1KHz or 1.5KHz, EMD-CLEAN method performs best; when the PRF $\geq$ 2KHz, our proposed Robust EMD-CLEAN method is superior to the other three methods. In addition, when the PRF is 1.5KHz, the classification accuracy of the turbojet aircraft obtained via EMD-CLEAN is 56%, which means that it is hard to effectively categorize the turbojet aircraft via EMD-CLEAN method with such low PRF. For Figure 6(c), the radar carrier frequency is 1.3GHz (L band), the PRF is 4KHz and the dwell time is 30ms. As shown in Figure 6(c), when the test SNR $\geq$ 10 dB, our Robust EMD-CLEAN method yields the best classification rates, all of which are higher than 80%. Comparing the Robust EMD-CLEAN method with the EMD-CLEAN method, we can see that the proposed noise reduction approach can significantly improve the classification accuracies especially when the test SNR $\leq$ 20 dB.

If we assume that the classification threshold is 80% in the simulated experiment, our Robust EMD-CLEAN method can work with the dwell time $\geq$ 20ms, the PRF $\geq$ 1.5KHz and under the test SNR $\geq$ 10 dB; the Robust EIG-SPECTRUM method requires the dwell time $\geq$ 20ms, the PRF $\geq$ 3KHz and the test SNR $\geq$ 15 dB; the Robust CLEAN method requires the dwell time $\geq$ 30ms, the PRF $\geq$ 2KHz and the test SNR $\geq$ 15 dB; the EMD-CLEAN method requires the dwell time $\geq$ 20ms, the PRF $\geq$ 1.5KHz and the test SNR $\geq$ 15 dB. Therefore, compared with the other three related methods, our proposed method can achieve the good classification performance not only with the lower PRF and the shorter dwell time but also under the lower test SNR condition, which means it is easier for an air defense radar system to accomplish the task of simultaneous detection and classification via our proposed classification scheme.

B. Experiment on Measured Data

In this experimental scheme, we utilize the simulated data in the training stage and the measured data in the classification stage to evaluate the performance of the four classification methods in the real application. This measured dataset is collected under high SNR condition. For aircraft-like targets under a look-up scenario such as the case of our experiment, the noises in the inphase and quadrature echoes of targets can be assumed to be Gaussian white noises. As discussed in Section I, since the test SNR condition is directly related to the classification distance, we add simulated white noise to the inphase and quadrature components of the raw complex measured data to evaluate the noise-robustness of the classification methods. Here the training data are still simulated

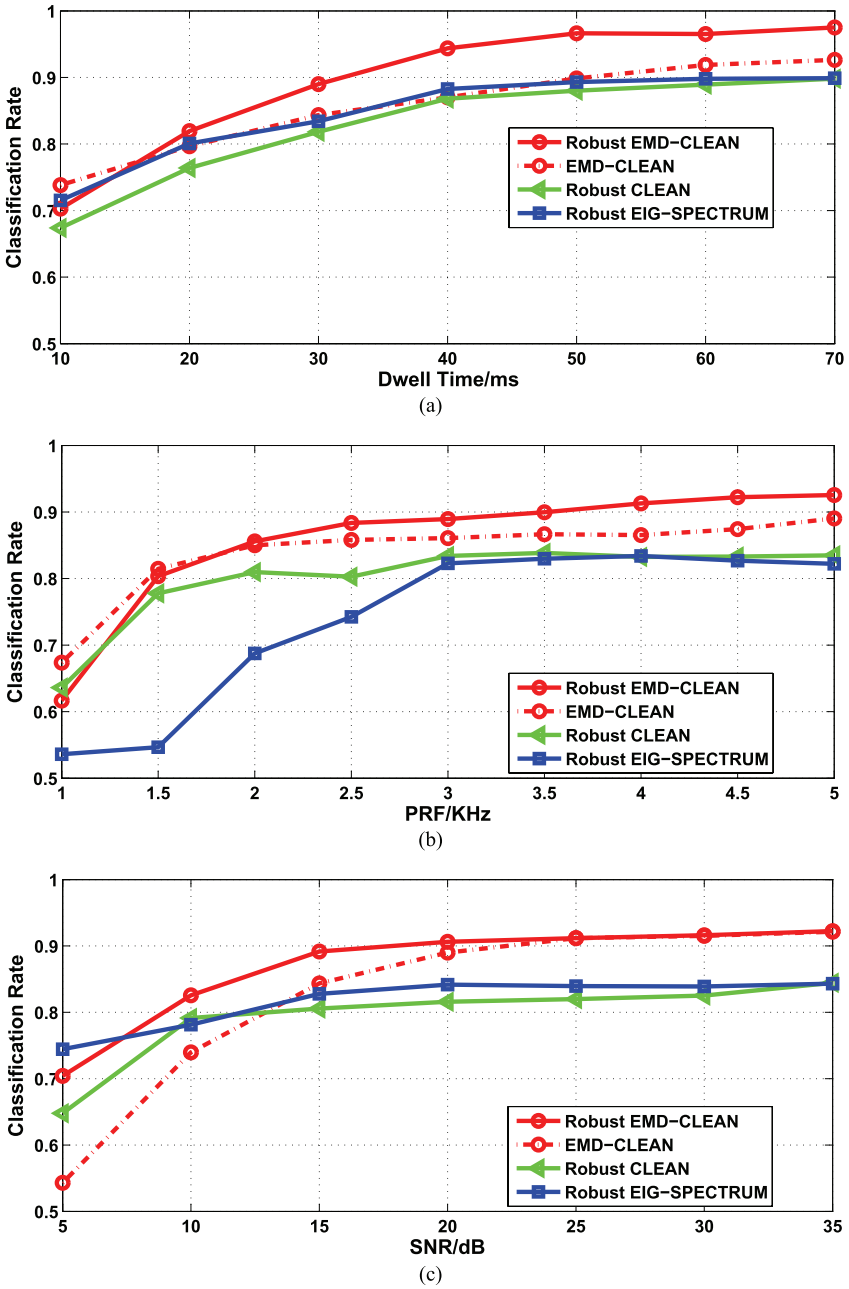

Fig. 6. Variation of the classification performance of the simulated data with the dwell time, PRF and test SNR, via Robust EMD-CLEAN, Robust EIG-SPECTRUM, Robust CLEAN and EMD-CLEAN. For each subfigure, given a set of radar or test condition parameters, there are one training set and three test sets (some flight conditions of the test aircrafts are different between the test sets) for all four classification methods, where the training data are simulated with the training aircraft models and without considering the noise effect, while the test data are simulated with the test aircraft models (different from the training models) and considering different SNR conditions. The classification rates are averaged over the three runs with the three test datasets. (a) Variation curves with the dwell time (L band, the PRF of 4KHz and the test SNR of 15 dB). (b) Variation curves with the PRF (L band, the dwell time of 30ms and the test SNR of 15 dB). (c) Variation curves with the test SNR (L band, the dwell time of 30ms and the PRF of 4KHz).

without noise, while the measured data with simulated noises are used as the test data.

Figure 7 deciptes the average classification rates versus the test SNR. We can see our proposed robust classification scheme, *i.e.*, Robust EMD-CLEAN always performs best in distinguishing the three kinds of aircrafts under the different test SNR conditions. Moreover, comparing the Robust EMD-CLEAN method with the EMD-CLEAN method, when the test SNR $\geq$ 30 dB, there is no significant difference between the performance of the two methods; when the test SNR $\leq$ 25 dB, the Robust EMD-CLEAN method can yield higher classification rates, which means that the proposed noise reduction approach can significantly improve the classification performance under the low SNR condition. If we assume that the classification threshold for the real application is 70%, our Robust EMD-CLEAN method can work under the test condition of SNR $>$ 10 dB; the EMD-CLEAN method and the Robust EIG-SPECTRUM method require the test SNR $>$ 15 dB; the Robust CLEAN method requires SNR $>$ 20 dB. Thus, according to the radar equation, the 5 dB or 10 dB

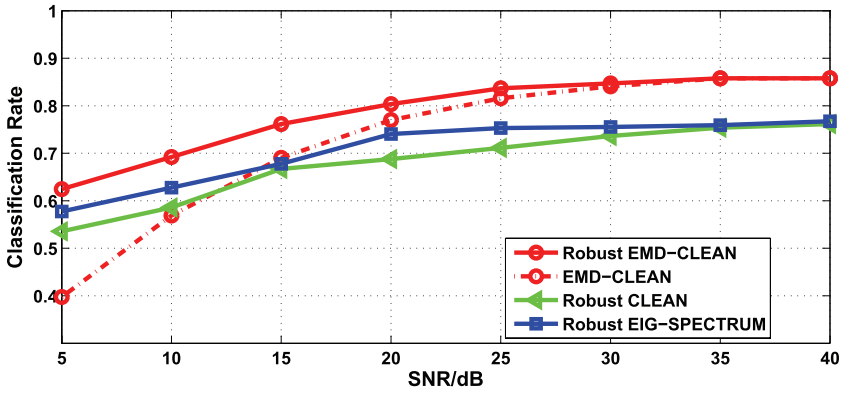

Fig. 7. Variation of the classification rates of the measured test data with the test SNR via Robust EMD-CLEAN, Robust EIG-SPECTRUM, Robust CLEAN and EMD-CLEAN. The training data are simulated without noise, while the measured data with simulated noises are used as the test data.

TABLE II

CLASSIFICATION ACCURACIES OF EACH AIRCRAFT CATEGORY (TURBOJET AIRCRAFT, PROP AIRCRAFT AND HELICOPTER) AND THE AVERAGE RATES VIA ROBUST EMD-CLEAN, ROBUST EIG-SPECTRUM AND ROBUST CLEAN UNDER THE HIGH TEST SNR CONDITION (SNR = 40 dB)

classification method	turbojet aircraft	prop aircraft	helicopter	average classification accuracy
Robust EMD-CLEAN	82.26%	92.71%	97.53%	86.33%
Robust EIG-SPECTURM	83.87%	62.33%	90.36%	77.35%
Robust CLEAN	79.03%	96.88%	50.62%	76.57%

advantage in SNR via our method can bring an increase about 30% or 60% in the classification distance between the target and radar in the real application.

Table II further compares the classification accuracies of each aircraft category and the average rates via Robust EMD-CLEAN, Robust EIG-SPECTRUM and Robust CLEAN under the high test SNR condition (SNR = 40 dB). From Table II, we can see, although the noises in the classification stage can be ignored in this case (*i.e.*, the proposed noise reduction approach cannot take effect in this case), the Robust EIG-SPECTRUM method (equivalent to the EIG-SPECTRUM method in this case) fails to categorize the prop aircraft effectively (its classification accuracy is just about 60%) and the Robust CLEAN method (equivalent to CLEAN method in this case) cannot categorize the helicopter effectively (its classification accuracy is just about 50%), while our Robust EMD-CLEAN method (equivalent to EMD-CLEAN method in this case) can categorize any aircraft of the three kinds into the right class with the accuracy over 80%.

VI. CONCLUSION

In this paper, we proposed a novel classification scheme to categorize airplane targets into three kinds, i.e., turbojet aircraft, prop aircraft and helicopter, based on the JEM characteristics of their low resolution radar echoes. The EMD method and CLEAN technique are used to separate the JEM component from the fuselage component, and we further extract the five-dimensional feature vector from the decomposition results of EMD and CLEAN. In order to improve the classification performance under the low test SNR condition, a simple and efficient preprocessing method is also proposed for the classification stage to denoise the received test sample. Experimental results based on the simulated and measured data show that the proposed classification scheme can obtain good classification performance not only with the relatively low PRF and the relatively short dwell time but also under the relatively low test SNR condition. Compared with the three related classification methods, the radar parameter and test condition requirements of our proposed classification scheme can be more easily met by an air defense radar system especially with the task of simultaneous detection and classification.

Here we only discuss the target classification problem with the low resolution returned echoes from the narrow band radar. Due to the low resolution, the narrow band radar system can only decide the initial categories of the targets. If we transmit some wide band signals to obtain the high resolution range profiles (HRRPs) after radar detects and initially classifies the target, we can further recognize the target model based on the radar HRRPs [13].

REFERENCES

[1] X. R. Bai, M. D. Xing, F. Zhou, G. Y. Lu, and Z. Bao, "Imaging of micromotion targets with rotating parts based on empirical-mode decomposition," *IEEE Trans. Geosci. Remote Sens.*, vol. 46, no. 11, pp. 3514–3522, Nov. 2008.

[2] M. R. Bell and R. A. Grubbs, "JEM modeling and measurement for radar target identification," *IEEE Trans. Aerosp. Electron. Syst.*, vol. 29, no. 1, pp. 73–87, Jan. 1993.

[3] S. Bjorklund, T. Johansson, and H. Petersson, "Evaluation of a micro-doppler classification method on mm-wave data," in *Proc. IEEE Radar Conf.*, May 2012, pp. 934–939.

[4] L. Bottou, C. Cortes, and J. S. Denker, "Comparison of classifier methods: A case study in handwriting digit recognition," in *Proc. IEEE Int. Conf. Pattern Recognit.*, Oct. 1994, pp. 77–87.

[5] C. J. Cai, W. X. Liu, J. S. Fu, and Y. L. Lu, "A new approach for ground moving target indication in foliage environment," *Signal Process.*, vol. 86, no. 1, pp. 84–97, Jan. 2006.
[6] C. J. Cai, W. X. Liu, J. S. Fu, and Y. L. Lu, "Radar micro-Doppler signature analysis with HHT," *IEEE Trans. Aerosp. Electron. Syst.*, vol. 46, no. 2, pp. 929–938, Apr. 2010.
[7] E. Candes, J. Romberg, and T. Tao, "Robust uncertainty principles: Exact signal reconstruction from highly incomplete frequency information," *IEEE Trans. Inf. Theory*, vol. 52, no. 2, pp. 489–509, Feb. 2006.
[8] F. Chen, H. W. Liu, L. Du, and Z. Bao, "Target classification with low-resolution radar based on diserpersion situations of eigenvalue spectra," *Sci. China Inf. Sci.*, vol. 53, no. 7, pp. 1446–1460, 2010.
[9] V. C. Chen, "Doppler signatures of radar backscattering from objects with micro motions," *IET Signal Process.*, vol. 2, no. 3, pp. 291–300, 2008.
[10] V. C. Chen, F. Li, S. S. Ho, and H. Wechsler, "Analysis of micro-Doppler signatures," *IEE Proc.-Radar Sonar Navigat.*, vol. 150, no. 4, pp. 271–276, Aug. 2003.
[11] V. C. Chen, F. Li, S. S. Ho, and H. Wechsler, "Micro-Doppler effect in radar: Phenomenon, model, and simulation study," *IEEE Trans. Aerosp. Electron. Syst.*, vol. 42, no. 1, pp. 2–21, Jan. 2006.
[12] D. Donoho, "Compressed sensing," *IEEE Trans. Inf. Theory*, vol. 52, no. 4, pp. 5406–5425, Apr. 2006.
[13] L. Du, H. W. Liu, P. H. Wang, B. Feng, M. Pan, F. Chen, and Z. Bao, "Noise robust radar HRRP target recognition based on multitask factor analysis with small training data size," *IEEE Trans. Signal Process.*, vol. 60, no. 7, pp. 3546–3559, Jul. 2012.
[14] M. Elshafei, S. Akhtar, and M. S. Ahmed, "Parametric models for helicopter identification," *IEEE Trans. Aerosp. Electron. Syst.*, vol. 36, no. 4, pp. 1242–1252, Oct. 2000.
[15] P. Flandrin, G. Rilling, and P. Goncalves, "Empirical mode decomposition as a filter bank," *IEEE Signal Process. Lett.*, vol. 11, no. 2, pp. 112–114, Feb. 2004.
[16] H. W. Gao, L. G. Xie, S. L. Wen, and Y. Kuan, "Micro-Doppler signature extraction from ballistic target with micro-motions," *IEEE Trans. Aerosp. Electron. Syst.*, vol. 46, no. 4, pp. 1969–1982, Oct. 2010.
[17] N. E. Huang, Z. Shen, and S. R. Long and, "The empirical mode decomposition and the hilbert spectrum for nonlinear and non-stationary time series analysis," *Proc. R. Soc. London*, vol. 454, no. 1971, pp. 903–995, 1998.
[18] K. Huo, Y. X. Liu, J. M. Hu, W. D. Jiang, and X. Li, "A novel imaging method for fast rotating targets based on the segmental pseudo keystone transform," *IEEE Trans. Geosci. Remote Sens.*, vol. 49, no. 4, pp. 1464–1472, Apr. 2011.
[19] Y. Kim and H. Ling, "Human activity classification based on micro-Doppler signatures using a support vector machine," *IEEE Trans. Geosci. Remote Sens.*, vol. 47, no. 5, pp. 1328–1337, May 2009.
[20] U. Kreoel, "Pairwise classification and support vector machines," in *Advances in Kernel Methods—Support Vector Learning*. Cambridge, MA, USA: MIT Press, 1999, pp. 255–268.
[21] N. Levanon and E. Mozeson, *Radar Signals*. New York, NY, USA: Wiley, 2004.
[22] X. Li, B. Deng, Y. L. Qin, H. Q. Wang, and Y. P. Li, "The influence of target micromotion on SAR and GMTI," *IEEE Trans. Geosci. Remote Sens.*, vol. 49, no. 7, pp. 2738–2751, Jul. 2011.
[23] Y. Luo, Q. Zhang, C. Qiu, X. J. Liang, and K. M. Li, "Micro-Doppler effect analysis and feature extraction in ISAR imaging with stepped-frequency chirp signals," *IEEE Trans. Geosci. Remote Sens.*, vol. 48, no. 4, pp. 2087–2098, Apr. 2010.
[24] G. J. Melendez and S. B. Kesler, "Spectrum estimation by neural networks and their use for target classification by radar," in *Proc. Int. Conf. Acoust., Speech, Signal Process.*, 1995, pp. 3615–3618.
[25] P. Molchanov, J. Astola, K. Egiazarian, and A. Totsky, "Classification of ground moving radar targets by using joint time-frequency analysis," in *Proc. IEEE Radar Conf.*, May 2012, pp. 366–371.
[26] J. A. Nanzer and R. L. Rogers, "Bayesian classification of humans and vehicles using micro-Doppler signals from a scanning-beam radar," *IEEE Microw. Wireless Compon. Lett.*, vol. 19, no. 5, pp. 338–340, May 2009.
[27] P. F. Pellegrini-S and C. S. Pardini, "Radar signals analysis oriented to target characterization applied to civilian atc radar," in *Proc. Int. Conf. Radar*, 1992, pp. 438–445.
[28] R. G. Raj, V. C. Chen, and R. Lipps, "Analysis of radar human gait signatures," *IET Signal Process.*, vol. 4, no. 3, pp. 234–244, 2010.
[29] S. S. Ram, C. Christianson, Y. Kim, and L. Hao, "Simulation and analysis of human micro-Dopplers in through-wall environments," *IEEE Trans. Geosci. Remote Sens.*, vol. 48, no. 4, pp. 2015–2023, Apr. 2010.
[30] G. Rilling, P. Flandrin, and P. Goncalves, "Bivariate empirical mode decomposition," *IEEE Signal Process. Lett.*, vol. 14, no. 12, pp. 936–939, Dec. 2007.
[31] M. Ruegg, E. Meier, and D. Nuesch, "Vibration and rotation in millimeter-wave SAR," *IEEE Trans. Geosci. Remote Sens.*, vol. 45, no. 2, pp. 293–304, Feb. 2007.
[32] M. I. Skolnik, *Radar Handbook*, 3 ed. New York, NY, USA: McGraw-Hill, 2008.
[33] G. E. Smith, K. Woodbridge, and C. J. Baker, "Naïve Bayesian radar micro-Doppler recognition," in *Proc. Int. Conf. Radar*, pp. 111–116, 2008.
[34] G. E. Smith, K. Woodbridge, and C. J. Baker, "Radar micro-Doppler signature classification using dynamic time warping," *IEEE Trans. Aerosp. Electron. Syst.*, vol. 46, no. 3, pp. 1078–1096, Jul. 2010.
[35] G. E. Smith, K. Woodbridge, C. J. Baker, and H. Griffiths, "Multistatic micro-Doppler radar signatures of personnel targets," *IET Signal Procss.*, vol. 4, no. 3, pp. 224–233, 2010.
[36] T. Sparr and B. Krane, "Micro-Doppler analysis of vibrating targets in SAR," *IEE Proc.-Radar Sonar Navigat.*, vol. 150, no. 4, pp. 277–283, Aug. 2003.
[37] L. Stankovic, I. Djurovic, and T. Thayaparan, "Separation of target rigid body and micro-Doppler effects in ISAR imaging," *IEEE Trans. Aerosp. Electron. Syst.*, vol. 42, no. 4, pp. 1496–1506, Oct. 2006.
[38] T. Tanaka and D. P. Mandic, "Complex empirical mode decomposition," *IEEE Signal Process. Lett.*, vol. 14, no. 2, pp. 101–104, Feb. 2007.
[39] T. Thayaparan, S. Abrol, E. Riseborough, L. Stankovic, D. Lamothe, and G. Duff, "Analysis of radar micro-doppler signatures from experimental helicopter and human data," *IET Radar, Sonar Navigat.*, vol. 1, no. 4, pp. 289–299, 2007.
[40] J. Tsao and B. D. Steinberg, "Reduction of sidelobe and speckle artifacts in microwave imaging: The clean technique," *IEEE Trans. Antennas Propag.*, vol. 36, no. 4, pp. 543–556, Apr. 1988.
[41] J. Weston and C. Watkins, "Multi-class support vector machines," in *Proc. ESANN*, Brussels, Belgium, 1999, pp. 63–70.
[42] Z. Xu, B. Huang, and F. Zhang, "Improvement of empirical mode decomposition under low sampling rate," *Signal Process.*, vol. 89, no. 11, pp. 2296–2303, 2009.
[43] B. Xuan, Q. W. Xie, and S. L. Peng, "EMD sifting based on bandwidth," *IEEE Signal Process. Lett.*, vol. 14, no. 8, pp. 527–540, Aug. 2007.
[44] Q. Zhang, T. S. Yeo, H. S. Tan, and Y. Luo, "Imaging of a moving target with rotating parts based on the Hough transform," *IEEE Trans. Geosci. Remote Sens.*, vol. 46, no. 1, pp. 291–299, Jan. 2008.

Lan Du (M'11) received the B.S., M.S., and Ph.D. degrees in electronic engineering from Xi'dian University, Xi'an, China, in 2001, 2004, and 2007, respectively. Her doctoral dissertation was granted Top 100 Doctoral Dissertation in China in 2009. From 2007 to 2009, she was a Post-Doctoral Research Associate with the Department of Electrical and Computer Engineering, Duke University, Durham, NC, USA. She is currently a Professor with the National Laboratory of Radar Signal Processing, Xi'dian University.

Her current research interests include statistical signal processing and machine learning with application to radar target recognition.

Baoshuai Wang received the B.Eng. degree in electrical and information engineering from Shandong Normal University, Jinan, China, in 2010. He is currently pursuing the Ph.D. degree in signal processing at the National Laboratory of Radar Signal Processing, Xi'dian University, Xi'an, China.

His current research interests include radar signal processing, radar automatic target recognition, and pattern recognition.

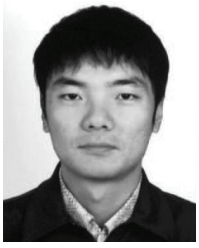

Yanbing Li received the B.Sc. degree in mechanical and electrical engineering from Chang'an University, Xi'an, China, in 2006, and the M.S. and Ph.D. degrees in signal processing from Xi'dian University, Xi'an, China, in 2009 and 2013, respectively.

His current research interests include radar signal processing, radar automatic target recognition, and pattern recognition.

Hongwei Liu (M'00) received the M.Eng. and Ph.D. degrees in electronic engineering from Xi'dian University, Xi'an, China, in 1995 and 1999, respectively. From 2001 to 2002, he was a Visiting Scholar with the Department of Electrical and Computer Engineering, Duke University, Durham, NC, USA. He is currently a Professor with the National Laboratory of Radar Signal Processing, Xi'dian University, and the Director of this laboratory.

His current research interests include radar signal processing, radar automatic target recognition, adaptive signal processing, and cognitive radar.